

## ESTIMATION OF SCATTERING CONTRIBUTION IN THE CALIBRATION OF NEUTRON DEVICES WITH RADIONUCLIDE SOURCES IN ROOMS OF DIFFERENT SIZES

by

**Rahim KHABAZ**

Physics Department, Faculty of Sciences, Golestan University, Gorgan, Iran

Scientific paper  
DOI: 10.2298/NTRP1501047K

Calibrations of neutron devices used in area monitoring are often performed by radionuclide neutron sources. Device readings increase due to neutrons scattered by the surroundings and the air. The influence of said scattering effects have been investigated in this paper by performing Monte Carlo simulations for ten different radionuclide neutron sources inside several sizes of concrete wall spherical rooms ( $R_{sp} = 200$  to 1500 cm). In order to obtain the parameters that relate the additional contribution from scattered neutrons, calculations using a polynomial fit model were evaluated. Obtained results show that the contribution of scattering is roughly independent of the geometric shape of the calibration room. The parameter that relates the room-return scattering has been fitted in terms of the spherical room radius, so as to reasonably accurately estimate the scattering value for each radionuclide neutron source in any geometry of the calibration room.

*Key words:* neutron, calibration, scattering contribution, radionuclide source, MCNPX

### INTRODUCTION

Instrument reading for any neutron irradiation varies with experimental conditions. One of the factors is the scattering by walls and air within the room. Quantifying the impact of this factor is important for facilities performing instrument calibrations [1-3].

Calibrations of neutron sensitive instruments are usually carried out by irradiating the device with a physically small neutron source of known energy and emission rate [4, 5]. Proper calibration procedures require that the instrument reading be corrected for all effects that may influence it, including neutron scattering by air, also known as room-return. The resulting calibration factor is independent of the characteristics of the calibration room, and the results are reproducible between different calibration facilities. Neutron room scattering corrections depend upon neutron source features, detector type, source-to-detector distance ( $l$ ), and calibration room configuration [6, 7].

For a point detector and a point source in an evacuated space, the product  $Ml^2$  is a constant, where  $M$  is the deadtime corrected count rate of the detector, induced by the source at a separation distance  $l$ . Since the calibrations are generally performed in small cali-

bration halls, and source neutrons scattered by the air within the room and reflected by the walls, this simple relationship has to be considerably modified [8, 9]. The general functional relationship for detector reading in open geometry,  $M(l)$ , as a function of the separation distance, is given by

$$M(l) = \frac{C}{l^2} \frac{F_1(l)}{F_A(l)} F_2(l) \quad (1)$$

where  $C$  is the source-detector combination characteristic constant, function  $F_1(l)$  – the geometry correction [10, 11],  $F_A(l)$  – the air attenuation (air outscatter) correction,  $F_2(l)$  – the correction function which describes the additional contribution from neutrons that can be represented by [12]

$$F_2(l) = 1 + A' l S l^2 \quad (2)$$

where  $S$  is the fractional room-scatter contribution at unit calibration distance, while  $A'$  is the air in-scattered component.

$F_A(l)$  can be given by a good approximation as [13]

$$F_A(l) = \frac{1}{1 + A' l} \quad (3)$$

For a point-like detector  $F_1(l) = 1$ , eq. (1) can, thus, be rewritten as

\* Corresponding author; e-mail: r.khabaz@gu.ac.ir

$$M(l) = \frac{C}{l^2} F_2(l) \quad (4)$$

where

$$F_2(l) = 1 - A/l - S/l^2 \quad (5)$$

and  $A$  is given by

$$A = A_1 - A_2 \quad (6)$$

In eq. (5),  $A/l$  is the total fractional component (inscatter minus outscatter) due to air scattering. The scattering factor  $F_2(l)$  can also be obtained from

$$F_2(l) = \frac{M_t(l)}{M_d(l)} - 1 = \frac{M_s(l)}{M_d(l)} \quad (7)$$

where  $M_t(l)$  is the total detector reading,  $M_s(l)$  – the detector reading due to scattered neutrons, and  $M_d(l)$  – the detector reading from source neutrons alone.

When the scattering effect is considered a complete data set of neutron spectra measurements, the function of distance in the calibration room can be used to have a better evaluation of those wall-returned neutrons. However, this solution is not always feasible, due to time-consuming efforts; thus, Monte Carlo calculations are commonly used to determine neutron scattering corrections [14].

The International Organization for Standardization recommends several radionuclide sources for the calibration of radiation protection measuring devices, with their own energy spectrum and mean energy ( $ME$ ), ranging from a few tenths to a few MeV [15-17]. However, in ideal conditions, the selection of the source to perform the calibration with should depend upon the neutron spectrum of the field in which the instrument is normally utilized and the variation of its response with the incident neutron energy.

The main goal of this paper is to investigate neutron transport inside concrete spherical rooms in order to determine the value of the scattering, as well as the features of parameters  $A$  and  $S$ . Thus, ten radionuclide neutron sources:  $^{241}\text{Am-Li}$ ,  $^{238}\text{Pu-Li}$ ,  $\text{Po-Be}$ ,  $^{241}\text{Am-F}$ ,  $^{252}\text{Cf}$ ,  $^{241}\text{Am-B}$ ,  $^{241}\text{Am-Be}$ ,  $\text{Ra-Be}$ ,  $^{239}\text{Pu-Be}$ , and  $^{242}\text{Cm-Be}$  [18], having different energy spectra, were placed in the center of seven 100 cm-thick concrete wall spherical cavities, whose radii are 200, 400, 500, 800, 1000, 1200, and 1500 cm, so as to determine the changes in the neutron spectra due to scattering in several  $l$  and, in addition, assess the parameters  $A$  and  $S$  for each of the configurations of the source room.

## MATERIALS AND METHODS

Nowadays, the Monte Carlo method is widely used for solving various scientific problems involving statistical processes and is particularly well-suited for medical physics and nuclear engineering applications, due to the stochastic nature of radiation emission, transport and detection processes. In the present work,

the Monte Carlo code MCNPX2.6 [19], with the latest cross-section library ENDF/B-VII.0 [20], was used to simulate the 100 cm-thick concrete spherical shell rooms. For the thermal domain, the  $S(\alpha, \beta)$  treatment was employed in the simulation. The  $S(\alpha, \beta)$  treatment takes into account the effect of chemical binding and crystalline structure during the scattering of thermal neutrons. The concrete density whose elemental composition was 0.6% H, 50.0% O, 1.7% Na, 4.8% Al, 31.5% Si, 1.9% K, 8.3% Ca, and 1.2% Fe amounted to 2.35 g/cm<sup>3</sup> [21]. In the model, a point-like neutron source was located at the center of the spherical room air and the detectors located at different distances from the source, up to a point located near the room's inner surface. The air features were dry, near sea level, with a density of 1.205 kg/cm<sup>3</sup>, with their element concentration considered to be 79.1% N and 20.9% O. The number of histories was large enough to reach a statistical error of less than 1% [22].

In the first step, the dependence of scattering due to the shape of the room was evaluated. In order to determine the behavior of the scattering value in terms of the room shape, calculations were done for the three room shapes, *i. e.*, spherical, cubical and rectangular parallelepiped. In these simulations, two sets of rooms with equal inner surface areas were studied. One set included a spherical room with a radius of 500 cm, a cubical room with dimensions of 723.60 cm, and a rectangular parallelepiped room with dimensions of 1017.33 cm × 700 cm × 500 cm; another set was constituted by a spherical room with a radius of 800 cm, a cubical room with dimensions of 1157.76 cm, and a rectangular parallelepiped room with dimensions of 1530.63 cm × 1200 cm × 800 cm. The inner surface area of these two sets was 314.16 m<sup>2</sup> and 804.25 m<sup>2</sup>, respectively.

Afterwards, seven different sizes of spherical rooms whose inner radii ( $R_{sp}$ ) are 200, 400, 500, 800, 1000, 1200, and 1500 cm were simulated. The radionuclide neutron source was supposed to be at the geometrical center of each room, and the detector at different distances along the spherical cavity radius. Numbers of these distances were considered from 10 to 20 situations depending on the size of the room. For each situation, using point detector tally (F5), the total fluence due to direct and scattered neutrons was determined.

By calculating the ratio of the total neutron fluence to the direct fluence for each source-to-detector distance ( $l$ ), the scattering correction factor,  $F_2(l)$ , is quantified. Then, by the fitting of these values as a function of  $l$  based on eq. (5), one can determine the  $A$  and  $S$  parameters for each neutron source and room size.

## RESULTS AND DISCUSSION

The calculated values of  $M_s(l)$  multiplied by the square of the source-to-detector distance,  $l$ , are plot-

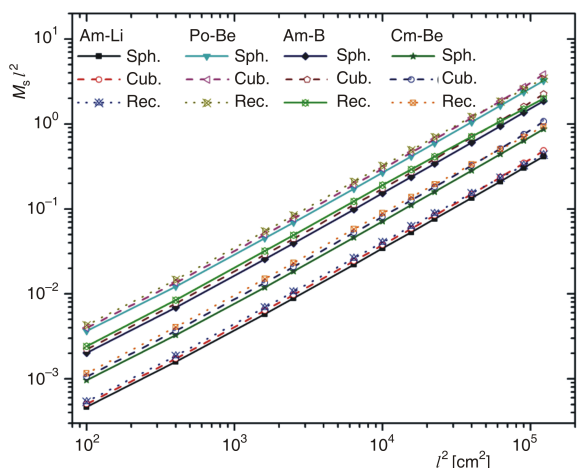


**Figure 1.** Comparison of the scattering fluence times the square of source-to-detector distance  $l$  for four neutron sources inside different room shapes with  $a = 314.16 \text{ m}^2$  (to prevent clutter, the results of Po-Be,  $^{241}\text{Am-B}$ , and  $^{242}\text{Cm-Be}$  have been multiplied by factors of 10, 8, and 5, respectively)

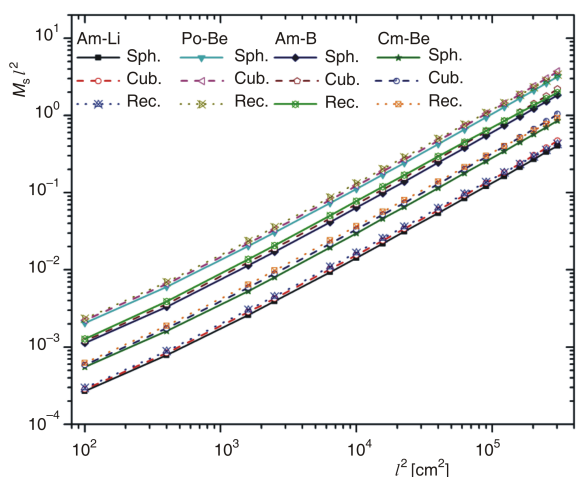


**Figure 2.** Comparison of the scattering fluence times the square of source-to-detector distance  $l$  for four neutron sources inside different room shapes with  $a = 804.25 \text{ m}^2$  (to prevent clutter, the results of Po-Be,  $^{241}\text{Am-B}$ , and  $^{242}\text{Cm-Be}$  have been multiplied by factors of 10, 8, and 5, respectively)

ted against  $l^2$  in fig. 1. This figure compares the fraction of scattering in three room shapes, *i. e.*, spherical, cubical, and rectangular parallelepiped, whose inner surface area ( $a$ ) is  $314.16 \text{ m}^2$  for the four radionuclide sources:  $^{241}\text{Am-Li}$  ( $ME = 0.56 \text{ MeV}$ ), Po-Be ( $ME = 2.04 \text{ MeV}$ ),  $^{241}\text{Am-B}$  ( $ME = 3.27 \text{ MeV}$ ), and  $^{242}\text{Cm-Be}$  ( $ME = 5.50 \text{ MeV}$ ) [18]. Figure 2 also presents the corresponding results for the three room shapes with  $a = 804.25 \text{ m}^2$ . In order to accommodate the presentation of twelve curves in a single figure and prevent clutter, the results of some sources have been multiplied by factors.

By comparing figs. 1 and 2, it can be observed that the scattering neutron fluence is far from  $1/l^2$  behavior; for the same  $l$  in a smaller room, there is also more room-return contribution in comparison with the larger room. Indeed, fewer neutrons hit the surfaces of the larger room per unit area than in the smaller one, which leads to a reduction in wall scattered fluence in the larger room. It can, thus, be noted that the scattering fluence is dependent on the inner surface area of the room, and that it is also approximately independent of its shape. The largest difference is for  $^{242}\text{Cm-Be}$  and for places where the detector is close to the wall, with the relative differences being less than 13%; however, for other points, it amounts to less than 8%.

Measured or computed neutron spectra are in most cases originally obtained as group fluences in energy bins. Each of the bins is described by its lower boundary,  $E_i$ , and its upper boundary,  $E_{i+1}$ . The group fluence in the  $i$ th energy bin is given by

$$\varphi_i = \int_{E_i}^{E_{i+1}} \Phi_E(E) dE \quad (8)$$

For graphical representation, the logarithm of neutron energy is used as the abscissa. In this case, it is an appropriate representation of the fluence per unit lethargy. Upon substituting  $\ln E$  for  $E$  in eq. (8), one obtains, again using the mean value theorem

$$\varphi_i = \frac{\int_{\ln E_i}^{\ln E_{i+1}} \Phi_E(E) d(\ln E)}{E_i \Phi_E(E) (\ln E_{i+1} - \ln E_i)} \quad (9)$$

From eq. (9), it is obvious that the appropriate ordinate for the representation of spectra is the group fluence in a bin divided by the difference in the logarithms of neutron energy, *i. e.*, by lethargy.

To compare the variations in the neutron fluence spectra, results of  $^{241}\text{Am-F}$  and Ra-Be as representative samples are plotted for the smallest and largest spherical room radii. These sources were selected because their mean source energies are 2.46 MeV and 4.78 MeV, respectively. In figs. 3 and 4, the  $^{241}\text{Am-F}$  neutron spectra in the rooms of 200 cm and 1500 cm radii are shown.

Here it can be noticed that for both rooms and for a small  $l$ , the spectra have similar shapes. As the  $l$  increases, the spectrum tends to become softer; however, in neutron energy ( $E_n$ ) below  $10^{-1} \text{ MeV}$  and  $10^{-3} \text{ MeV}$ , the fluence remains approximately constant at all  $l$  for 200 cm and 1500 cm-radius rooms, respectively.

By comparing the spectra at 100 cm in the 200 cm-radius room with the corresponding spectrum in the 1500 cm-radius room, the maximum fluence (in  $E_n = 3.5 \text{ MeV}$ ) is 12 times greater in the smaller room compared with the larger cavity, which also appears to be softer.

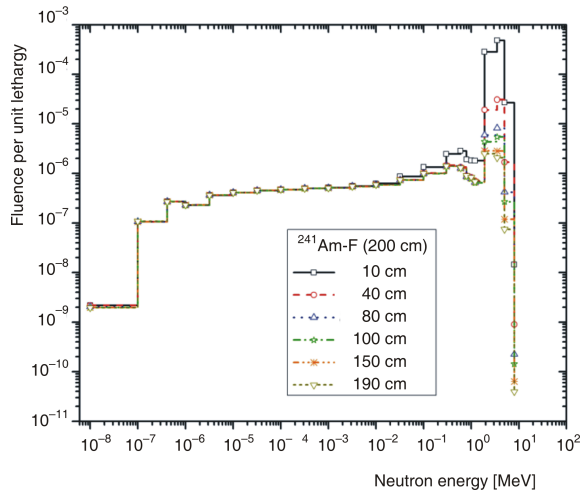


**Figure 3.**  $^{241}\text{Am-F}$  neutron spectrum, at different source-to-detector distances, inside a 200 cm-radius concrete room

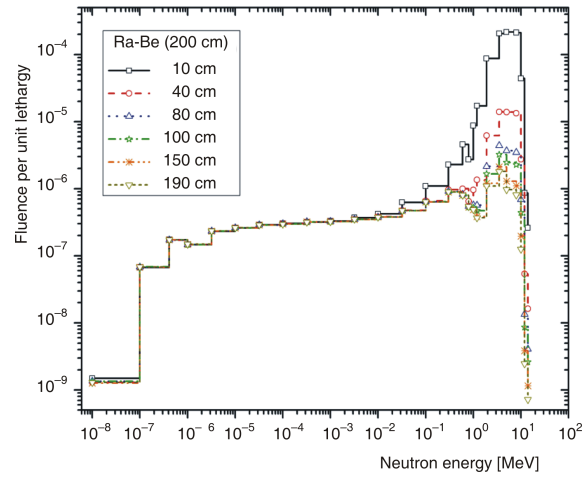


**Figure 5.** Neutron spectra of Ra-Be inside a 200 cm-radius concrete room at different source-to-detector distances

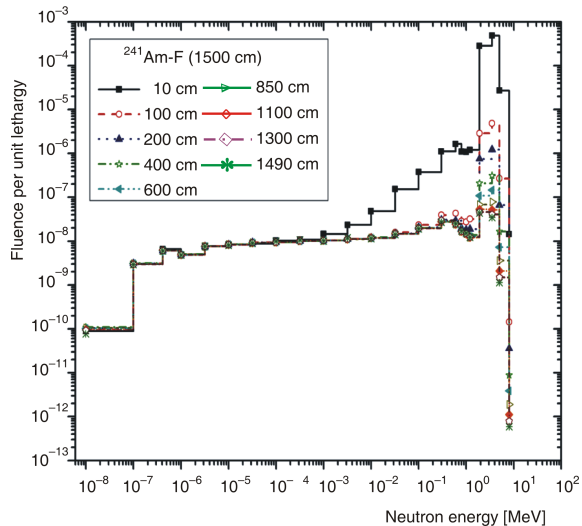


**Figure 4.**  $^{241}\text{Am-F}$  neutron spectrum, at different source-to-detector distances, inside a 1500 cm-radius concrete room

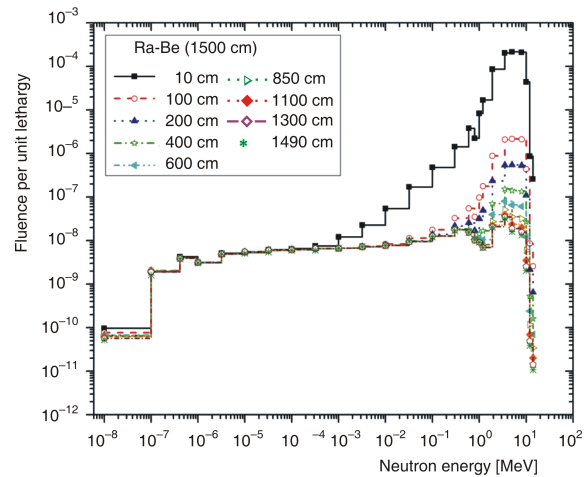


**Figure 6.** Neutron spectra of Ra-Be inside a 1500 cm-radius concrete room at different source-to-detector distances

In figs. 5 and 6, the Ra-Be neutron spectra at various  $l$  are also shown in the smallest and the largest radius rooms.

These figures show that for energies of  $10^{-7}$  to  $2 \cdot 10^{-3}$  MeV in a 200 cm-radius room and  $10^{-7}$  to  $2 \cdot 10^{-4}$  MeV in a 1500 cm-radius room, the spectra have a similar shape at all distances; however, for both rooms in other energies, as the  $l$  increases, the fluence of Ra-Be decreases. For the same  $l$  in the smaller room, the total neutron fluence of Ra-Be is greater; however, this increase is less in comparison to the  $^{241}\text{Am-F}$  source. For example, the fluence of Ra-Be at 100 cm in the 200 cm-radius room, for  $E_n = 3.5$  MeV, is only about 1.5 times greater than the corresponding fluence in the 1500 cm-radius room.

In figs. 5 and 6, the behavior of the fluence of the Ra-Be source at low energies is similar to the  $^{241}\text{Am-F}$  source, since both do not emit neither epithermal nor thermal neutrons; however, the concrete cavity due to room return creates the epithermal and thermal neutron fluence.

Using the Monte Carlo simulation inside seven sizes of a spherical concrete cavity, the correction factor  $F_2(l)$  was obtained based on eq. (7) at different distances for ten radionuclide neutron sources. These calculations were performed for  $10^7$  histories which provided a reasonable statistical error. The range of relative statistical errors for the total detector reading in the simulations of each neutron source is given in tab. 1.

**Table 1. Range of relative errors obtained from calculations of each neutron source**

Neutron source	Range of relative error [%]
<sup>241</sup> Am-Li	0.007-0.91
<sup>238</sup> Pu-Li	0.007-0.92
Po-Be	0.008-0.98
<sup>241</sup> Am-F	0.005-0.85
<sup>252</sup> Cf	0.01-0.98
<sup>241</sup> Am-B	0.01-0.90
<sup>241</sup> Am-Be	0.02-0.94
Ra-Be	0.006-0.82
<sup>239</sup> Pu-Be	0.006-0.92
<sup>242</sup> Cm-Be	0.01-0.92

The results for any room size were fitted based on eq. (5), and parameters *A* and *S* were calculated for each neutron source. The achieved values of parameters *A* and *S* are listed in tabs. 2 and 3, respectively. For all sources, the values of parameter *S* from tab. 3 were plotted as a function of the room size in fig. 7.

It can be observed that the value of parameter *A* is negative, except for two sources, *i. e.*, <sup>238</sup>Pu-Li and Ra-Be, inside the 1500 cm-radius spherical room. Based on eq. (6), having a positive value of *A* means that inscattering by the air is greater than outscattering, and *vice versa*.

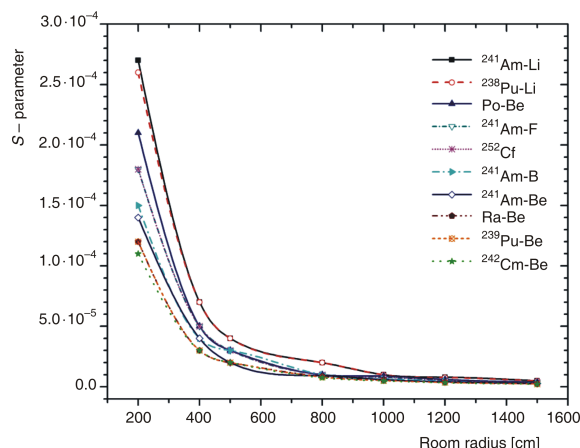


**Figure 7. Parameter *S* of the  $F_2(l)$  vs. the room's radii for different neutron sources**

Here, the *S* value decreases as the room size increases, and in each room size it varies for each neutron source. This is because of the fact that in the smaller room there are more neutrons scattered by walls in comparison with the larger one.

This figure illustrates an inverse square dependence of parameter *S* values to the radius of the spherical room. In other words, parameter *S* varies with the inner surface area of the room; however, it is inde-

**Table 2. Parameter *A* of eq. (5) for the best fit of the calculated fractional component of scattering vs. the source-to-detector distance (*l*), for the different radionuclide neutron sources inside seven spherical rooms**

Neutron source ( <i>ME</i> )	200 cm	400 cm	500 cm	800 cm	1000 cm	1200 cm	1500 cm
<sup>241</sup> Am-Li (0.56 MeV)	-1.46E-03*	-7.10E-04	-6.10E-04	-3.10E-04	-2.60E-04	-1.80E-04	-2.00E-05
<sup>238</sup> Pu-Li (0.60 MeV)	-1.25E-03	-5.60E-04	-4.70E-04	-2.60E-04	-2.20E-04	-8.00E-05	+3.00E-05
Po-Be (2.04 MeV)	-1.09E-03	-3.80E-04	-4.10E-04	-1.40E-04	-1.50E-04	-7.00E-05	-3.00E-05
<sup>241</sup> Am-F (2.46 MeV)	-9.90E-04	-5.00E-04	-3.60E-04	-2.00E-04	-2.00E-04	-1.10E-04	-2.00E-05
<sup>252</sup> Cf (2.54 MeV)	-8.90E-04	-4.80E-04	-3.00E-04	-2.10E-04	-1.90E-04	-7.00E-05	-2.00E-05
<sup>241</sup> Am-B (3.27 MeV)	-7.30E-04	-3.50E-04	-4.10E-04	-1.50E-04	-1.60E-04	-1.30E-04	-5.00E-05
<sup>241</sup> Am-Be (4.46 MeV)	-7.50E-04	-4.10E-04	-3.10E-04	-1.80E-04	-1.80E-04	-1.10E-04	-7.00E-05
Ra-Be (4.78 MeV)	-7.20E-04	-3.50E-04	-3.10E-04	-2.10E-04	-1.60E-04	-9.00E-05	+1.00E-05
<sup>239</sup> Pu-Be (5.40 MeV)	-7.10E-04	-3.70E-04	-2.30E-04	-1.30E-04	-9.00E-05	-1.00E-04	-5.00E-05
<sup>242</sup> Cm-Be (5.50 MeV)	-7.40E-04	-3.90E-04	-2.70E-04	-1.40E-04	-1.00E-04	-7.00E-05	-5.00E-05

\*Read as  $-1.46 \cdot 10^{-3}$

**Table 3. Parameter *S* of eq. (5) for the best fit of the calculated fractional component of scattering vs. the source-to-detector distance (*l*), for the different radionuclide neutron sources inside seven spherical rooms**

Neutron source ( <i>ME</i> )	200 cm	400 cm	500 cm	800 cm	1000 cm	1200 cm	1500 cm
<sup>241</sup> Am-Li (0.56 MeV)	2.700E-04	7.000E-05	4.000E-05	2.000E-05	1.000E-05	7.832E-06	4.902E-06
<sup>238</sup> Pu-Li (0.60 MeV)	2.600E-04	7.000E-05	4.000E-05	2.000E-05	1.000E-05	7.592E-06	4.779E-06
Po-Be (2.04 MeV)	2.100E-04	5.000E-05	3.000E-05	1.000E-05	8.762E-06	6.038E-06	3.873E-06
<sup>241</sup> Am-F (2.46 MeV)	1.800E-04	5.000E-05	3.000E-05	1.000E-05	7.690E-06	5.286E-06	3.350E-06
<sup>252</sup> Cf (2.54 MeV)	1.800E-04	5.000E-05	3.000E-05	1.000E-05	7.905E-06	5.396E-06	3.451E-06
<sup>241</sup> Am-B (3.27 MeV)	1.500E-04	4.000E-05	3.000E-05	9.893E-06	6.447E-06	4.519E-06	2.868E-06
<sup>241</sup> Am-Be (4.46 MeV)	1.400E-04	4.000E-05	2.000E-05	9.101E-06	5.913E-06	4.083E-06	2.638E-06
Ra-Be (4.78 MeV)	1.200E-04	3.000E-05	2.000E-05	8.484E-06	5.454E-06	3.752E-06	2.327E-06
<sup>239</sup> Pu-Be (5.40 MeV)	1.200E-04	3.000E-05	2.000E-05	8.021E-06	5.127E-06	3.631E-06	2.316E-06
<sup>242</sup> Cm-Be (5.50 MeV)	1.100E-04	3.000E-05	2.000E-05	7.459E-06	4.786E-06	3.336E-06	2.161E-06

**Table 4. Fitting coefficient  $G$  for the achieved parameter  $S$  vs. room radius for each source**

Neutron source (ME)	$G$ – coefficient
$^{241}\text{Am-Li}$ (0.56 MeV)	10.811 0.081
$^{238}\text{Pu-Li}$ (0.60 MeV)	10.445 0.099
Po-Be (2.04 MeV)	8.350 0.082
$^{241}\text{Am-F}$ (2.46 MeV)	7.251 0.080
$^{252}\text{Cf}$ (2.54 MeV)	7.251 0.081
$^{241}\text{Am-B}$ (3.27 MeV)	6.060 0.099
$^{241}\text{Am-Be}$ (4.46 MeV)	5.633 0.086
Ra-Be (4.78 MeV)	4.808 0.023
$^{239}\text{Pu-Be}$ (5.40 MeV)	4.807 0.016
$^{242}\text{Cm-Be}$ (5.50 MeV)	4.439 0.053

pendent of room geometry. Therefore, parameter  $S$  was fitted as a function of the radius of spherical rooms by

$$S = G \frac{Q}{R_{sp}^2} \quad (10)$$

where  $G$  is a coefficient,  $Q$  – the neutron emission rate, and  $R_{sp}$  – the radius of the room. In MCNPX code, the calculation was performed for  $Q = 1$ .

The obtained values of coefficient  $G$  from fitting by the least square technique are listed in tab. 4 for each neutron source. The fitting was done using Origin version 8 software. It can be seen that the coefficient  $G$  decreases with an increase in the mean energy of the neutron source.

In order to evaluate the accuracy of this fitting, the values of scattering achieved by eq. (10) and obtained by Monte Carlo simulation were compared. As an example, for four different sources inside a 700 cm-radius room, the calculated values of  $M_s(l)$  multiplied by the square of the source-to-detector distance are plotted against  $l^2$  in fig. 8. The room was simulated without air, so as to assess only the contribution of room scattering. Using eqs.(5) and (10) in eq. (7) and considering  $A = 0$ , the detector reading due to scattered neutrons can be obtained from

$$M_s(l) = \frac{G}{R_{sp}^2} l^2 M_d(l) \quad (11)$$

By inserting  $M_d(l)$  based on the inverse square law, the above equation may be rewritten as

$$M_s(l) = \frac{G}{4\pi R_{sp}^2} l^2 \quad (12)$$

It can be seen that the agreement between the amount of scatterings obtained from fitting eq. (12) and Monte Carlo simulations are quite good, bearing in mind that, for the  $^{241}\text{Am-Be}$  source, the difference is relatively higher; however, the largest difference is less than 6%.

Thus, eqs. (5) and (10) can provide a reasonable estimate for the room-return scattering in any size of a

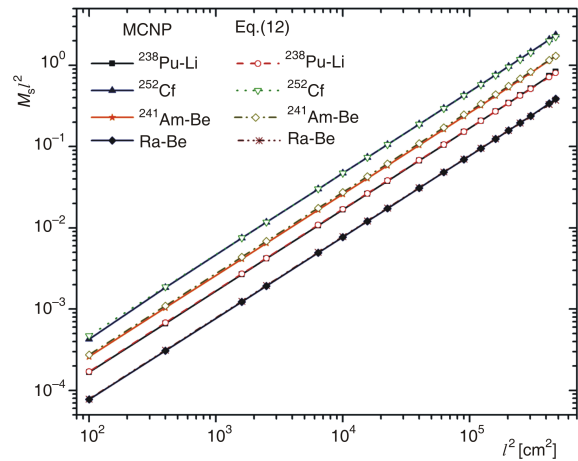


**Figure 8. Comparison of the scattering fluence times the square of source-to-detector distance  $l$  for four neutron sources inside a 700 cm-radius room obtained from MCNPX calculation and eq. (12) (to prevent clutter, the results of  $^{252}\text{Cf}$  and  $^{241}\text{Am-Be}$  have been multiplied by factors of 4 and 3, respectively)**

spherical room. Furthermore, based on the independence of room-return scattering from the room geometric shape (figs. 1 and 2), these relations can apply to any calibration room having an inner surface area equal to the area of a specific spherical cavity.

## CONCLUSIONS

A Monte Carlo study has been performed to evaluate the effect of 100-cm-thick concrete spherical rooms on the neutron spectra of  $^{241}\text{Am-Li}$ ,  $^{238}\text{Pu-Li}$ , Po-Be,  $^{241}\text{Am-F}$ ,  $^{252}\text{Cf}$ ,  $^{241}\text{Am-B}$ ,  $^{241}\text{Am-Be}$ , Ra-Be,  $^{239}\text{Pu-Be}$ , and  $^{242}\text{Cm-Be}$  radionuclide neutron sources. The calculations were carried out for spectra at different source-to-detector distances in cavities containing air with radii of 200, 400, 500, 800, 1000, 1200, and 1500 cm. The results were used to achieve the room-scattered component,  $S$ , and air-scattered component,  $A$ , for each source-room configuration.

There is strong evidence of the independence of the room-return scattering contribution from the geometric shape of the calibration room, the difference between the scattering contribution of spherical, cubical and rectangular parallelepiped rooms being less than 13%; however, the scattering value is approximately equal for different rooms having the same inner area surface.

Furthermore, the room-scattering component,  $S$ , has been fitted as a function of the inverse square of radius (surface area) of the spherical room. The difference between the scattering contribution obtained from MCNPX simulation and fitting equations for a 700 cm-radius room was less than 6%.

Therefore, the proposed equations, along with the listed parameters and coefficients, can be viewed

as a viable tool for assessing and quantifying the contribution of scattering for each radionuclide neutron source in any geometry of a calibration room.

#### ACKNOWLEDGMENT

This work was supported by the Golestan University (Iran) under contract of Research Project No. 93/71/19861.

#### REFERENCES

- [1] Khabaz, R., Analysis of Neutron Scattering Components Inside a Room with Concrete Walls, *Applied Radiation and Isotopes*, 95 (2015), pp. 1-7
- [2] Vega-Carrillo, H. R., *et al.*, Study of Room-Return Neutrons, *Radiation Measurements*, 42 (2007), 3, pp. 413-419
- [3] Vega-Carrillo, H. R., *et al.*, Spectrum of Isotopic Neutron Sources Inside Concrete Wall Spherical Cavities, *Radiation Measurements*, 42 (2007), 8, pp. 1373-1379
- [4] Khabaz, R., Miri, H., Development of a Bonner Sphere Spectrometer with Emphasis on Decreasing the Contribution of Scattering by Using a New Designed Shadow Cone, *Journal of Radioanalytical and Nuclear Chemistry*, 289 (2011), 3, pp. 789-794
- [5] Khabaz, R., Miri, H., Measurement of Neutron Spectrum with Multi-Sphere Using BF<sub>3</sub> and Evaluation of Scattering Effect on Spectrum, *Nucl Technol Radiat*, 26 (2011), 2, pp. 140-146
- [6] Eisenhauer, C. M., Schwartz, R. B., Johnson, T., Measurement of Neutrons Reflected from the Surfaces of a Calibration Room, *Health Physics*, 42 (1982), 4, pp. 489-495
- [7] Eisenhauer, C. M., Review of Scattering Corrections for Calibration of Neutron Instruments, *Radiation Protection Dosimetry*, 28 (1989), 4, pp. 253-262
- [8] Hunt, J. B., The Calibration of Neutron Sensitive Spherical Devices, *Radiation Protection Dosimetry*, 8 (1984), 4, pp. 239-251
- [9] Liu, J. C., Hajnal, F., Sims, C. S., Kuiper, J., Neutron Spectral Measurements at ORNL, *Radiation Protection Dosimetry*, 30 (1990), 3, pp. 169-178
- [10] Khabaz, R., Examining the Departure in Response of Non-Point Detectors Due to Non Uniform Illumination and Displacement of Effective Center, *Nuclear Instruments and Methods A*, 728 (2013), pp. 145-149
- [11] Khabaz, R., Investigation of the Effects of Beam Divergence on the Response of Neutron Voluminous Detectors, *Journal of Radioanalytical and Nuclear Chemistry*, 300 (2014), 3, pp. 91-917
- [12] Kluge, H., Weise, K., Hunt, J. B., Calibration of Neutron Sensitive Spherical Devices with Bare and D<sub>2</sub>O-Moderated <sup>252</sup>Cf Sources in Rooms of different sizes, *Radiation Protection Dosimetry*, 32 (1990), 4, pp. 233-244
- [13] Eisenhauer, C. M., Hunt, J. B., Schwartz, R. B., Calibration Techniques for Neutron Personal Dosimetry, *Radiation Protection Dosimetry*, 10 (1985), 1-4, pp. 43-57
- [14] Yoon, S. C., *et al.*, Determination of Neutron Room Scattering Corrections in RCL's Calibration Facility at KAERI, *Radiation Protection Dosimetry*, 70 (1997), 1-4, pp. 349-351

- [15] \*\*\*, ISO 8529-3, Reference Neutron Radiations – Part 3: Calibration Fundamentals of Radiation Protection Devices Related to the Basic Quantities Characterizing the Radiation Field, International Organization for Standardization, 56. CH-1211, Geneva, 1998
- [16] \*\*\*, ISO 8529-2, Reference Neutron Radiations – Part 2: Calibration Fundamentals of Radiation Protection Devices Related to the Basic Quantities Characterizing the Radiation Field, International Organization for Standardization, 56. CH-1211, Geneva, 2000
- [17] \*\*\*, ISO 8529-1, Reference Neutron Radiations – Part 1: Characteristic and Methods of Productions, International Organization for Standardization, 56, CH-1211, Geneva, 2001
- [18] Griffith, R. V., Palfalvi, J., Madhvanath, U., Compendium of Neutron Spectra and Detector Responses for Radiation Protection Purposes, International Atomic Energy Agency Technical Report Series No. 318, Vienna, 1990
- [19] \*\*\*, MCNPX-A General Monte-Carlo N-Particle Transport Code: Version 2.6, LANL Report, LA-CP-07-1473, Los Alamos, (Ed. Pelowitz, D. B.), 2008
- [20] Chadwick, M. B., *et al.*, ENDF/BVII.0: Next Generation Evaluated Nuclear Data Library for Nuclear Science and Technology, *Nuclear Data Sheets*, 107 (2006), 12, pp. 2931-3060
- [21] Harmon, Ch. D., *et al.*, Criticality Calculations with MCNP-TM: A Primer, Los Alamos National Laboratory Report LA-12827-M, 1994
- [22] Seltzer, S. M., Berger, M. J., Evaluation of the collision Stopping Power of Elements and Compounds for Electrons and Positrons, *International Journal of Applied Radiation Isotopes*, 33 (1982), 11, pp. 1189-1218

Received on September 8, 2014

Accepted on January 30, 2015

**Рахим КАБАЗ**

**ПРОЦЕНА ДОПРИНОСА РАСЕЈАНОГ ЗРАЧЕЊА КАЛИБРАЦИЈИ  
НЕУТРОНСКИХ УРЕЂАЈА ПОМОЋУ РАДИОАКТИВНИХ ИЗВОРА У  
ПРОСТОРИЈАМА РАЗЛИЧИТИХ ДИМЕНЗИЈА**

Калибрација неутронских уређаја за мониторинг средине често се обавља помоћу радиоактивних извора неутрона, имајући у виду при томе да су читавања уређаја увећана услед расејаних неутрона из околине и ваздуха. Тема овог рада је утицај расејаног зрачења који је истражен обављеним Монте Карло симулацијама за десет различитих неутронских извора унутар сферичних просторија различитих димензија ( $R_{sp} = 200$  cm до 1500 cm) са бетонским зидовима. За прорачуне коришћен је модел полиномијалног фитовања, како би се добили параметри који се односе на допринос расејаних неутрона. Добијени резултати показују да допринос расејаног зрачења битно не зависи од геометрије калибрационе просторије. Параметар који се односи на расејање из околине фитован је према полупречнику сферичне собе, како би се довољно прецизно могла проценити вредност расејаног зрачења за сваки радиоактивни извор неутрона у било којој геометрији калибрационе просторије.

*Кључне речи: неутрон, калибрација, допринос расејању, радиоактивни извор, MCNPX*

---